Growth of β-Amyloid(1−40) Protofibrils by Monomer Elongation and Lateral Association. Characterization of Distinct Products by Light Scattering and Atomic Force Microscopy†

Michael R. Nichols,‡ Melissa A. Moss,‡ Dana Kim Reed,‡ Wen-Lang Lin,‡ Rajendrani Mukhopadhyay,§ Jan H. Hoh,§ and Terrone L. Rosenberry*,‡

Department of Neurosciences, Mayo Clinic, 4500 San Pablo Road, Jacksonville, Florida 32224, and Departments of Pathology and Physiology, Johns Hopkins University School of Medicine, 725 North Wolfe Street, Baltimore, Maryland 21205

Received November 27, 2001; Revised Manuscript Received March 4, 2002

ABSTRACT: Amyloid plaques in brain tissue are a hallmark of Alzheimer's disease. Primary components of these plaques are 40- and 42-residue peptides, denoted Aβ(1−40) and Aβ(1−42), that are derived by proteolysis of cellular amyloid precursor protein. Synthetic Aβ(1−40) and Aβ(1−42) form amyloid fibrils in vitro that share many features with the amyloid in plaques. Soluble intermediates in Aβ fibrillogenesis, termed protofibrils, have been identified previously, and here we describe the in vitro formation and isolation of Aβ(1−40) protofibrils by size exclusion chromatography. In some experiments, the Aβ(1−40) was radiomethylated to better quantify various Aβ species. Mechanistic studies clarified two separate modes of protofibril growth, elongation by monomer deposition and protofibril−protofibril association, that could be resolved by varying the NaCl concentration. Small isolated protofibrils in dilute Tris-HCl buffers were directed along the elongation pathway by addition of Aβ(1−40) monomer or along the association pathway by addition of NaCl. Multi-angle light scattering analysis revealed that protofibrils with initial molecular masses M_w of (7−30) × 10^3 kDa grew to M_w values of up to 250 × 10^3 kDa by these two growth processes. However, the mass per unit length of the associated protofibrils was about 2−3 times that of the elongated protofibrils. Rate constants for further elongation by monomer deposition with the elongated, associated, and initial protofibril pools were identical when equal number concentrations of original protofibrils were compared, indicating that the original number of protofibril ends had not been altered by the elongation or association processes. Atomic force microscopy revealed heterogeneous initial protofibrils that became more rodlike following the elongation reaction. Our data indicate that protofibril elongation in the absence of NaCl results from monomer deposition only at the ends of protofibrils and proceeds without an increase in protofibril diameter. In contrast, protofibril association occurs in the absence of monomer when NaCl is introduced, but this association involves lateral interactions that result in a relatively disordered fibril structure.

Proteins form amyloid aggregates in a number of diseases. The brains of patients with Alzheimer's disease (AD)[1] contain large numbers of amyloid deposits in the form of senile plaques (*1*). The amyloid core of these plaques is composed of interwoven fibrils, each 7−9 nm in diameter (*2*), that can be visualized by light microscopy after staining with Congo Red or thioflavin (*3*). The fibrils in senile plaques are composed of 40- and 42-residue peptides (*4, 5*), denoted Aβ(1−40) and Aβ(1−42), that are derived by proteolysis of cellular amyloid precursor protein (APP) (*6*−*9*).

It has been difficult to establish whether Aβ peptides, amyloid fibrils, and the senile plaques in which they are found are important in the etiology of AD. Evidence that a higher Aβ peptide level is an important risk factor has come from studies of mutant genes that give rise to inherited forms of early-onset AD. These mutations, which occur in the genes for the APP or the presenilins (PS1 and PS2), all result in elevated levels of Aβ(1−42) (*10*). Furthermore, overexpression of these mutant genes in transgenic mice results in an age-dependent development of Aβ fibril deposition (*11, 12*). Fibrillar forms of Aβ appear to initiate a cascade of events that result in neuronal cell death and lead to the cognitive decline characteristic of AD (*13*). Therefore, therapeutic strategies that prevent fibril formation are attractive, and development of such strategies requires more insight into fibril formation and structure. In particular, characterization of intermediates in Aβ aggregation and clarification of how

† This work was supported by an award from the American Heart Association, Florida/Puerto Rico Affiliate (to M.R.N.), and by a sponsored research grant from Bristol-Myers Squibb Co. (to T.L.R.).

* To whom correspondence should be addressed. Telephone: 904-953-7375. Fax: 904-953-7370. E-mail address: rosenberry@mayo.edu.

‡ Mayo Clinic.

§ Johns Hopkins University School of Medicine.

[1] Abbreviations: AD, Alzheimer's disease; AFM, atomic force microscopy; DLS, dynamic light scattering; EM, electron microscopy; FPLC, fast performance liquid chromatography; MALS, multi-angle light scattering; PBS, phosphate-buffered saline; SEC, size exclusion chromatography; STEM, scanning transmission electron microscopy.

10.1021/bi015985r CCC: $22.00
Published on Web 04/17/2002

they progress to mature fibrils may identify new sites of action for inhibitors.

Aβ fibrillogenesis in vitro has been described as a nucleation-dependent polymerization process (*14, 15*) in which "monomeric" Aβ associates noncovalently to form nuclei or "seeds" from which soluble protofibrils and then full-length insoluble fibrils arise. The mechanism of Aβ nucleation and the structure of the nucleus are unknown, but a number of reports have investigated the physical and kinetic properties of fibrils and protofibrils. Both of these aggregated Aβ species possess an ordered, substantially β-sheet structure as determined by circular dichroism analysis (*16, 17*), and both have been reported to be toxic to neurons (*17*−*19*). Protofibril lengths (typically <200 nm; *15, 20*) are clearly less than the lengths of fibrils, which can exceed 1 mm (*21*), but differences in diameters are less clear. EM studies report widths of 6−10 nm (*15*) and 8.5 ± 1.5 nm (*22*) for Aβ(1−40) protofibrils and of 7−9 nm (*23*), 6−10 nm (*24*), and 9−12 nm (*22*) for Aβ(1−40) fibrils. AFM (*20*) and EM (*15*) have provided images of protofibrils that show a smaller, less rigid structure than the longer, rodlike fibrils.

The transient appearance of protofibrils precedes that of fibrils during Aβ aggregation in vitro, and this has suggested that protofibrils are precursors to fibrils (*25*). However, the mechanism of this transformation is not completely clear. Kinetic studies indicate that monomers deposit onto fibrils with a rate proportional to both fibril and monomer concentration (*26, 27*), and the same first-order dependence of deposition rate on monomer concentration has been reported with protofibrils (*28*). Direct association of protofibrils has been less rigorously investigated but also appears to play a role in fibril formation (*17, 28*). In this study, we show that protofibril growth by monomer deposition and direct association can be distinguished by structural analysis and ionic strength dependence. Estimation of protofibril size is an important feature of our analysis, and both dynamic light scattering (DLS) and static multi-angle light scattering (MALS) techniques were employed.

EXPERIMENTAL PROCEDURES

Materials. Aβ(1−40) peptide was obtained from QCB (Hopkinton, MA). [^{3}H]HCHO and [^{14}C]HCHO were from NEN Dupont, scintillation cocktail (Ultima Gold) was from Packard, and Sepharose CL-2B, EDTA, bovine serum albumin, and thioflavin T were from Sigma (St. Louis, MO).

Preparation of Aβ Peptide. Aβ(1−40) peptide was obtained in lyophilized form and stored at −20 °C desiccated until reconstitution in deionized water (18 MΩ; Millipore Milli-Q system) at 2.5 mg/mL (577 μM). Aliquots were flash-frozen in ethanol/dry ice, stored at −80 °C, and thawed at room temperature when needed. Stock solutions, stored for several weeks at 4 °C, retained their characteristic single-peak elution profiles corresponding to monomeric Aβ when examined by SEC on Superdex 75. Concentrations of monomeric Aβ were determined with a calculated extinction coefficient of 1450 cm^{-1} M^{-1} at 276 nm for the Aβ(1−40) peptide containing one tyrosine residue (*29*), and this value was confirmed by quantitative amino acid analysis (Beckman, System 6300).

Radiomethylation of Aβ(1−40). Reductive methylation of Aβ(1−40) was adopted from the procedure of Means (*30*). [^{3}H]HCHO (98 mCi/mmol) or [^{14}C]HCHO (54 mCi/mmol) (NEN DuPont) was used directly or after dilution to lower specific activity with unlabeled HCHO. Aβ(1−40) peptide (350 μM), 10 mM [^{3}H]- or [^{14}C]HCHO, 50 mM $NaCNBH_3$, and 10 mM sodium phosphate (pH 7) were incubated at room temperature for 3 h. The reaction was quenched by addition of 0.2 volume of 5 M Tris-HCl (pH 8.0), and labeled Aβ was separated from excess HCHO and side reaction products by SEC on Superdex 75. Radioactivity was determined by scintillation counting. Amino acid analysis (*31*) confirmed that the ϵ-amino groups of two lysine residues and the α-amino group of the N-terminal residue were converted to labeled dimethylamines, as expected for complete methylation of residues Asp1, Lys16, and Lys28 in Aβ(1−40), and established the specific activity of the labeled Aβ, which ranged from 1 to 1300 dpm/pmol.

Fluorescence Determinations of the Binding of Thioflavin T to Aβ Amyloid. Thioflavin T fluorescence determinations were made as described previously (*17, 32, 33*). Fluorescence was monitored by diluting Aβ samples into comparable buffer containing 5 μM thioflavin T at 23 °C on a Perkin-Elmer LS-50B luminescence spectrometer with excitation at 450 nm, emission from 470 to 500 nm, and excitation and emission slits of 10 nm. The area under the emission curve was obtained by integration and expressed as area units (F). Time drive experiments were conducted in a similar fashion with continuous monitoring of 480 nm fluorescence emission.

Liquid Chromatography. SEC employed two systems. Most molecular mass separations (0 to >20 kDa) were carried out with a 1 × 30 cm Superdex 75 HR 10/30 column (Amersham Pharmacia) attached to either a Pharmacia LKB or an AKTA FPLC system. The Superdex columns were washed with 1 M NaOH and pretreated with a bolus (50 mg) of BSA in running buffer to block nonspecific binding of Aβ protofibrils to the resin. Columns were then equilibrated in 5 or 50 mM Tris-HCl, 5 mM EDTA-NaOH (pH 8.0) (denoted 5 or 50 mM Tris−EDTA) containing 0−150 mM NaCl and run at a flow rate of 0.5 mL/min. Separations requiring slightly higher yields of high molecular mass aggregates employed a 0.6 × 28 cm Sepharose CL-2B column (Sigma) equilibrated in 50 mM Tris−EDTA with 0.05% BSA and run by hydrostatic pressure at a flow rate of 0.25 mL/min.

Aggregation of Aβ(1−40) to Protofibrils and Fibrils. Samples of unlabeled or radiomethylated Aβ(1−40) (70−100 μM) were incubated in 0.5−1 mL of 5 or 50 mM Tris−EDTA and 0−150 mM NaCl at room temperature and, unless otherwise noted, agitated vigorously by continued vortexing or platform shaking to promote aggregation (*34*−*36*). Incubation of purified radiomethylated Aβ(1−40) in the absence of EDTA for more than 1 day resulted in partial conversion to smaller peptide fragments (data not shown). This conversion was prevented by inclusion of 5 mM EDTA, so EDTA was included in all experiments. Aggregation was monitored by thioflavin T fluorescence, and the sample was microfuged for 10 min in a tabletop centrifuge (Beckman Coulter) at 18000*g* when a fluorescence increase estimated to be 20−100% of the maximum final fluorescence was observed. The pellet obtained from this centrifugation was defined as the fibril fraction. The supernatant was chromatographed on Superdex 75, and Aβ eluting in the void volume

was defined as the protofibril fraction. Protofibril elution was monitored by UV absorbance at 280 nm, thioflavin T fluorescence, and (with radiolabeled preparations) scintillation counting. The fluorescence profile superimposed precisely on the absorbance profile. However, concentrations determined from the apparent absorbance were corrected for light scattering by a conversion factor determined with radiolabeled protofibrils (see Figure 3 below). In most cases, isolated protofibrils were analyzed or committed to growth reactions immediately, but in a few cases, they were stored at 4 °C for up to 3 days before use.

Electron Microscopy (EM). Samples of Aβ fibrils and protofibrils were applied to 200 mesh Formvar-coated copper grids (Ernest F. Fullam, Inc., Latham, NY) and incubated for 2 min at room temperature. The sample was then wicked off with lens paper, and the grid was placed sample-side-down on a droplet of 0.5% gluteraldehyde (Sigma, diluted in filtered water). After 1 min, the fixative was wicked off and the grid washed with 5 droplets of filtered water. The sample side of the grid was placed down on a droplet of 2% uranyl acetate (Polysciences, Inc., Warrington, PA, dissolved in filtered water) and incubated for 1−5 min, after which the stain was wicked off and the grid was air-dried. Grids were visualized in a Philips EM208S transmission electron microscope. To estimate widths of individual strands in fibrils and protofibrils, photographs or negatives were scanned for analysis by AIS (Analytical Imaging System 4.0 Rev. 1.8 for Windows NT, Imaging Research Inc.). Using the "lane analysis" tool, longitudinal fibril segments were resolved into single strands or multiple parallel strands; then widths were measured as the average distance between parallel deposits of stain along the sides of each strand.

Dynamic Light Scattering (DLS). Hydrodynamic radius (R_H) measurements were made at room temperature with a DynaPro MSX instrument (Protein Solutions Inc., Charlottesville, VA) containing a gallium aluminum arsenide laser. Samples (60 μL) were placed directly into a quartz cuvette, and light scattering intensity at a 90° angle was collected using a 5 s acquisition time. Particle translational diffusion coefficients (D_T) were calculated from auto-correlated light intensity data (usually 20−25 points) and converted to R_H with the Stokes−Einstein equation ($R_H = k_bT/6\pi\eta D_T$). A histogram of percent intensity vs R_H was calculated using Dynamics data analysis software (Protein Solutions), and intensity-weighted mean R_H values were obtained for each subpeak.

Multi-angle Light Scattering (MALS). Analysis of light scattering data was based on the Zimm formalism of the Rayleigh−Debye−Gans model (*37*, *38*), which relates the excess Rayleigh ratio R_θ to the molecular structure according to eq 1:

$$\frac{Kc}{R_\theta} = \frac{1}{MP(\theta)} + 2A_2c \tag{1}$$

where R_θ is proportional to the fraction of incident light that is scattered by the solute without interference; K is a physical constant equal to $4\pi^2(dn/dc)^2n_o^2N_A^{-1}\lambda_o^{-4}$, where n is the refractive index of the solution, c is the solute concentration (g/mL), n_o is the refractive index of the solvent, N_A is Avogadro's number, and λ_o is the wavelength of the incident light in a vacuum; A_2 is the second virial coefficient; and M is the molecular mass of the solute. At the low concentrations c employed in this study, the $2A_2c$ term in eq 1 may be ignored. The function $P(\theta)$ is the ratio of the scattered light intensity to the scattered light intensity without interference. $P(\theta)$ equals 1 for small solute molecules, but for larger molecules whose size approaches λ_o, it increases to 1 only in the limit as θ, the angle between the incident and the scattered light, approaches zero. The reciprocal $P^{-1}(\theta)$ may be expressed by the power series in eq 2:

$$P^{-1}(\theta) = 1 + \frac{q^2R_g^{\,2}}{3} + ... \tag{2}$$

where $q = (4\pi n_o/\lambda_o)\sin(\theta/2)$ and R_g is the root-mean-square radius of gyration. According to eqs 1 and 2, a Zimm plot of Kc/R_θ as a polynomial in q^2 gives $(M)^{-1}$ as the y axis intercept and $R_g^2/3M$ as the limiting slope as θ approaches zero. In general, this plot remains linear in q^2 only for $qR_g < 1$, and curvature at higher qR_g depends on both the shape and the polydispersity of the molecules. For long rigid rod molecules of length L, $R_g = L/\sqrt{12}$ and $P(\theta)$ is given by eq 3 (*39*):

$$P(x) = \frac{2}{x}\int_0^x \frac{\sin z}{z}\,dz - \left[\frac{\sin(x/2)}{x/2}\right]^2 \tag{3}$$

where $x = qL$. For semiflexible wormlike chains, $P(\theta)$ is given by the expression developed by Koyama (*40*) in eq 4:

$$P(q) = \frac{2}{L_c^{\,2}}\int_0^{L_c}(L_c - t)\varphi(t,l_k,q)\,dt \tag{4}$$

where L_c is the contour length of the chain, l_k is the Kuhn statistical segment length, and the function φ is defined elsewhere (*40*); see (*41*). When the ratio $l_k/L_c \gg 1$, the chain is infinitely stiff and behaves as a rigid rod, with eq 4 reducing to eq 3.

When the solute is polydisperse, eqs 1 and 2 can still be applied if it is recognized that M in eq 1 becomes the weight average molecular mass M_w (eq 5a) and R_g in eq 2 becomes the mean square z-average radius of gyration R_{gz} (eq 5b):

$$M_w = \sum_{i=1}^{N} w_iM_i \tag{5a}$$

$$R_{gz}^{\,2} = \frac{\sum_i w_iM_iR_{gi}^{\,2}}{\sum_i w_iM_i} \tag{5b}$$

where w_i is the weight fraction of molecules with molecular mass M_i (*42*). Polydispersity of larger molecules complicates shape analysis with eqs 3 and 4 because $P(\theta)$ also varies with size, and eq 1 must be extended to eq 6:

$$\frac{R_\theta}{Kc} = \sum_i w_iM_iP_i(\theta) \tag{6}$$

The effect of polydispersity can be assessed if a solute distribution function is incorporated into eq 6 (*42*). We

applied a Flory distribution function predicted by a bifunctional polycondensation model (*43*, *44*) given in eq 7:

$$w_i(p) = i(1-p)^2 p^{(i-1)} \quad (7)$$

where $w_i(p)$ is the weight fraction of the ith polymer made of i monomers and $0 < p < 1$ represents the conversion degree of the monomers. Since M_i is proportional to i, eq 7 was used to generate an N-bin distribution of $M_w(N)$, with each bin representing a w_i of $1/N$ and the value $M_w(N)$ of each bin defined relative to that of the first bin $M_w(1)$. This w_i and these $M_w(N)$ were then inserted into eq 6, and $P_i(\theta)$ was taken from eq 4 with the assumption that $M_w(N)/L_c(N)$ and l_k were constant for all N (*44*). The resulting eq 6 was then fitted to experimental data with the numerical integration program SCoP (version 3.51) developed at the NIH National Center for Research Resources and available from Simulation Resources, Inc. (Redlands, CA) (*45*). Three parameters [$M_w(1)$, $L_c(1)$, and l_k] were varied to obtain the best fit for $N = 1$, 10, or 20.

When the length L of rigid rod molecules becomes large ($qL > 3.8$; *44*), Casassa (*46*) showed that Kc/R_θ for polydisperse solutes approaches a linear dependence on q as shown in eq 8:

$$\frac{Kc}{R_\theta} = \frac{2}{\pi^2}\frac{\sum_i w_i M_i/L_i^2}{(\sum_i w_i M_i/L_i)^2} + \frac{4\sin(\theta/2)}{\lambda' \sum_i w_i M_i/L_i} + \ldots \quad (8)$$

where $M_L = \Sigma w_i M_i/L_i$, the weight average mass per unit length. Thus, the slope of a plot of Kc/R_θ vs q approaches $(\pi M_L)^{-1}$ at high q. A similar limiting slope has been derived for semiflexible wormlike chains if both qL and $ql_k > 3.8$ (*44*, *47*).

Aβ protofibrils were separated by SEC in-line with a DAWN EOS multi-angle light scattering instrument (Wyatt Technology, Santa Barbara) employing incident light from a 30 mW gallium aluminum arsenide laser ($\lambda_o = 690$ nm). Eluted samples were passed through a K5 quartz flow cell surrounded by an array of 18 photodetectors at fixed angles normalized with bovine serum albumin (*44*). Scattered light at detectors 4−16 (corresponding to scattering angles of 26−143°), after correction for the refractive index of the glass and solvent, was recorded every 2 s during the column elution. Data for each 2 s interval were plotted according to eqs 1 and 2, usually with a third-order polynomial fit, to obtain values of M_w and R_{gz}. $R_{90°}$ was calibrated for the instrument with toluene as a solvent reference, and the value of dn/dc was taken as 0.186 cm^3/g (*48*). Additional procedural details were similar to those outlined elsewhere (*48*, *49*).

Protofibril Elongation/Association Assay. Protofibrils isolated on Superdex 75 were diluted to 1−2 μM (in Aβ residue units) in 50 mM Tris−EDTA with SEC-purified Aβ monomer (30 μM) (for elongation) or with 150 mM NaCl (for association) or without either addition and incubated without agitation at room temperature. In all elongation reactions, protofibrils and monomer were either both unlabeled or both labeled. Incubations of unlabeled protofibrils ranged from 20 to 120 min, while those of radiomethylated protofibrils were maintained for 3−22 h. Aliquots of the reaction were mixed with thioflavin T at the given time points if thioflavin T was excluded from the reaction, or thioflavin T fluorescence was continuously monitored in situ if thioflavin T was included in the reaction. Elongation rates were determined by linear regression of the initial increase in thioflavin T fluorescence.

Atomic Force Microscopy (AFM). Samples of Aβ protofibrils (100 μL) were incubated for 15 min at room temperature on freshly cleaved 15 mm disks of ruby muscovite mica (Asheville-Schoonmaker, Newport News, VA) modified with 3′-aminopropyl-triethoxy-silane (APTES) essentially as previously described (*50*). The mica disk was gently rinsed with water and blown dry with compressed gas. Care was taken to ensure that the disk remained dry once the sample preparation had been completed. A Nanoscope III controller with a Multimode AFM (Digital Instruments, Santa Barbara, CA) was used for imaging. Silicon cantilevers (TESP, Digital Instruments) were cleaned by exposure to high-intensity UV light (UVO Cleaner, Jelight Co. Inc., Laguna Hills, CA) for 20 min prior to use. Samples were imaged by ambient tapping mode AFM at scan speeds of 1−2 Hz, and 5 μm × 5 μm images were obtained (512 × 512 pixels). Particle height distributions were obtained with NanoScope (R) III (version 5.13r5, Digital Instruments), which displayed heights vs line distance on a horizontal or vertical line section through the image. Measured heights were assumed to be proportional to the particle diameters. The height distributions were related to M_L (eq 8) as follows: The probability n'_i of tabulating a particle with height h_i increases with the length of the particle L_i and is given by $n'_i = n_i L_i$, where n_i is the total number of particles with height h_i. Assuming that M_i is proportional to the molecular volume $\pi L_i h_i^2/4$ and given by $M_i = N_A \pi L_i h_i^2/4 \upsilon_p$ where υ_p is the partial specific volume of the particle, the relationship between M_L and h_i is given by eq 9. Defining $\langle h^2\rangle_w = \Sigma n'_i h_i^4/\Sigma n'_i h_i^2$, M_i/L_i for a specific population with height h_i is given by eq 10:

$$M_L = \frac{\sum_i c_i M_i/L_i}{\sum_i c_i} = \frac{\sum_i n_i M_i^2/L_i}{\sum_i n_i M_i} = \frac{N_A \pi \sum_i n'_i h_i^4}{4\upsilon_p \sum_i n'_i h_i^2} \quad (9)$$

$$M_i/L_i = M_L\left(\frac{h_i^2}{\langle h^2\rangle_w}\right) \quad (10)$$

RESULTS

Radiomethylation of and Purification of Aβ(1−40). Studies of Aβ aggregation can be complicated if monomeric Aβ stocks are contaminated by preexisting aggregates. To ensure that aggregation reactions were initiated with monomeric Aβ(1−40), we first resolved monomer from any residual aggregates by size exclusion chromatography (SEC) on Superdex 75 (*25*) (Figure 1A). The elution volume from this column has been reported to correspond to a molecular mass of 5−15 kDa relative to globular protein standards (*15*, *27*), but translational diffusion measurements by NMR indicated that the eluted Aβ corresponded to a monomer (4.3 kDa) (*27*). To better quantify Aβ in some experiments, we radiolabeled Aβ(1−40) by reductive radiomethylation (*30*). This

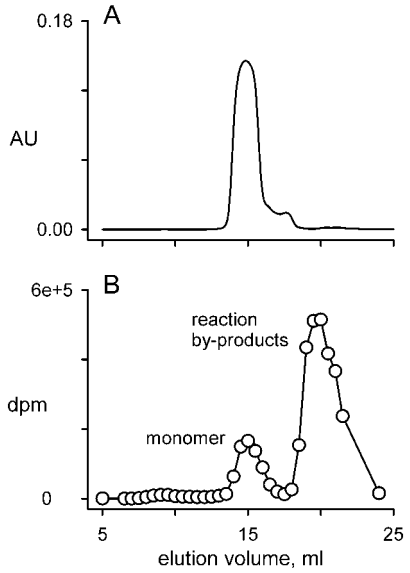

FIGURE 1: SEC of Aβ(1−40) peptide. Panel A: Unlabeled Aβ-(1−40) peptide was solubilized as outlined under Experimental Procedures and applied to Superdex 75 equilibrated in 50 mM Tris-HCl, 5 mM EDTA (pH 8.0) (50 mM Tris−EDTA). Peptide absorbance at 280 nm was monitored (AU). Panel B: Aβ(1−40) was reductively radiomethylated with [^{3}H]CHO as described under Experimental Procedures and applied to Superdex 75 as in panel A. Fractions were collected, and radioactivity (DPM) was determined by scintillation counting. Labeled Aβ(1−40) in the elution peak at 15 mL was resolved from labeled reaction by-products eluting in the later peak at 20 mL.

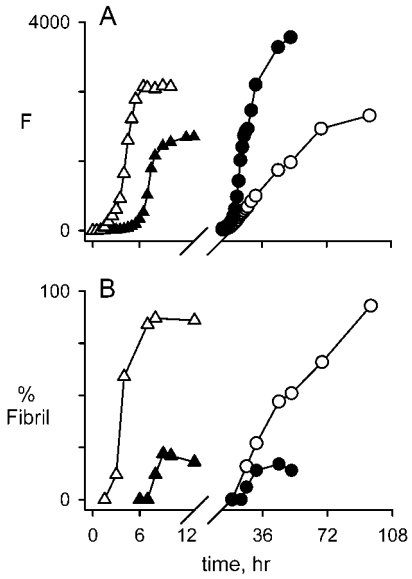

FIGURE 2: Aggregation of monomeric Aβ(1−40). Solutions of 70 μM Aβ(1−40) (triangles) or 70 μM [^{3}H]Aβ(1−40) (circles) in 50 mM Tris−EDTA containing either 150 mM (open symbols) or 40 mM NaCl (closed symbols) were agitated by continuous platform shaking at ~600 rpm. Panel A: Thioflavin T fluorescence (*F*) was measured as described under Experimental Procedures by mixing 10 μL aliquots of each Aβ(1−40) sample with 5 μM thioflavin T (200 μL) at the indicated times. Panel B: Aliquots from each sample (50 μL) were centrifuged at 18000*g* for 10 min, and the thioflavin T fluorescence remaining in the supernatant was measured. The percentage of Aβ(1−40) fibril formed was calculated as the percentage of total fluorescence lost in the supernatant.

reaction converted the primary amino groups at Asp1, Lys16, and Lys28 to ([^{3}H]- or [^{14}C]dimethyl)amines. Labeled Aβ-(1−40) was purified as the initial peak of radioactivity on Superdex 75 (Figure 1B). It eluted at the same volume as unlabeled Aβ(1−40) in Figure 1A and was well resolved from residual radioactive reagents and by-products in later fractions. Dynamic light scattering (DLS), previously used to characterize monomeric and oligomeric Aβ species (*15, 16, 51*), verified the absence of Aβ oligomers following SEC. Average hydrodynamic radius (R_H) values for purified preparations of unlabeled and labeled Aβ monomer were the same (1.4 ± 0.2 nm, SD, $n = 12$). Data in following sections indicate that radiomethylated Aβ(1−40) aggregated more slowly but formed protofibrils and fibrils that were virtually indistinguishable from unlabeled Aβ(1−40).

Aβ(1−40) Aggregation. Aggregation of radiolabeled and unlabeled monomeric Aβ(1−40) was induced by continuous agitation at two concentrations of NaCl and monitored with thioflavin T, a fluorophore that shows greatly enhanced fluorescence on binding to amyloid fibrils (*32*). The time course of aggregation was characterized by a delay, or lag time, that is well-known for amyloidogenic proteins (Figure 2A). The duration of the lag time is highly dependent on several factors, including monomer concentration and the initial presence of trace amounts of aggregates that can act as "seeds" (discussed in *52*). Unlabeled Aβ(1−40) solutions containing the lower 40 mM NaCl concentration displayed longer lag times than those with 150 mM NaCl (Figure 2A). Under equivalent conditions, radiomethylated Aβ(1−40) showed increased lag times compared to unlabeled Aβ(1−40), and the lag time sensitivity to NaCl concentration was not as evident (Figure 2A). Maximum fluorescence levels obtained with these four samples showed slight differences, but analysis of additional aggregation reactions indicated that these differences were not significant (data not shown).

Aliquots of the aggregating Aβ(1−40) samples in Figure 2A were periodically microfuged to sediment larger aggregates. Electron micrographs of the sedimented material revealed fibrils that were morphologically indistinguishable for the radiolabeled and the unlabeled samples (data not shown). However, the higher NaCl concentration had a striking effect in increasing the percentage of thioflavin T binding material that formed fibrils. Greater than 80% of the aggregates that bound thioflavin T were sedimented with 150 mM NaCl, while less than 20% were sedimented with 40 mM NaCl (Figure 2B). Furthermore, the time delay between the appearance of thioflavin T binding species and fibril formation at the higher NaCl concentration was very short, while a large percentage of the species that bound thioflavin T remained soluble in the supernatant at 40 mM NaCl even after no further aggregation was apparent. We have operationally defined these soluble aggregates that bind thioflavin T as protofibrils, and it is evident that the yield of protofibrils is increased at lower salt concentrations. Although DLS provides a very sensitive measure of aggregation, we were unable to detect significant levels of aggregates prior to the point at which fluorescence increases were observed in Figure 2. The initial rise in fluorescence was accompanied by the appearance of particles with average R_H values of 40−50 nm, and smaller aggregates were not observed. To compensate for the more rapid aggregation of unlabeled Aβ(1−40), we adjusted the ionic strength of reaction mixtures to generate protofibrils of similar size. Lag times and recoveries of protofibrils from unlabeled Aβ(1−40) were

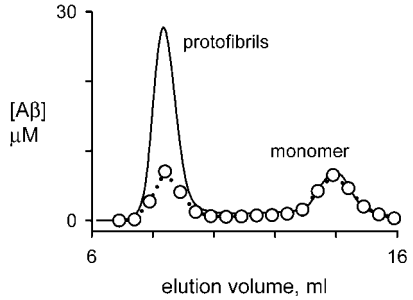

FIGURE 3: SEC of Aβ(1−40) protofibrils. [^{3}H]Aβ(1−40) (60 μM) was aggregated in 60 mM NaCl with vortex agitation at ∼2000 rpm under conditions otherwise identical to those in Figure 2, and after 18 h, the supernatant (0.8 mL) was applied to Superdex 75 equilibrated in 50 mM Tris−EDTA. Protofibrils eluting in the void volume (7.5−9.5 mL) were resolved from monomer in the partially included volume (13−15 mL). Elution was monitored by absorbance at 280 nm (line) and radioactivity (circles, dotted line) and converted to Aβ residue concentrations (μM) with an ϵ_{280nm} of 1450 cm^{-1} M^{-1} and the determined specific radioactivity. Recovery of radioactivity in eluted fractions was 49% of the onput.

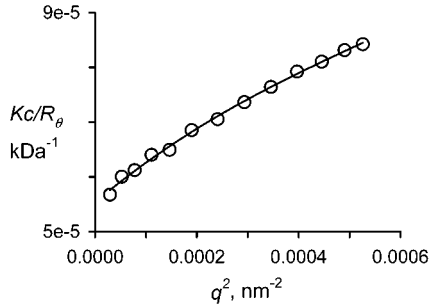

FIGURE 4: MALS analysis of Aβ(1−40) protofibrils. A 75 μL sample of [^{3}H]Aβ(1−40) protofibrils isolated as in Figure 3 was diluted to 500 μL and applied to Superdex 75 equilibrated in 50 mM Tris−EDTA and in-line with a DAWN EOS MALS unit (see Experimental Procedures). Light scattering data from detectors 4−16 were fitted to a Zimm plot as outlined in eqs 1 and 2. The plot shown corresponded to a 2 s interval (17 μL) at 7.6 mL of the protofibril elution peak. Extrapolation of this plot to $\theta = 0$ gave $M_w = 18 \times 10^3$ kDa and $R_{gz} = 65$ nm. For 35 intervals taken across the peak, from 50% of the maximum height on the leading edge to 75% of the maximum height on the trailing edge (7.3−7.9 mL), analysis with eqs 1 and 2 gave $M_w = 18 \pm 3$ (SD) $\times 10^3$ kDa and $R_{gz} = 63 \pm 10$ (SD) nm. If the protofibrils are assumed to be rigid rods (see text), their z-average length $L_z = \sqrt{12} \times R_{gz} = 218$ nm, and $M_w/L_z = 82$ kDa/nm.

further increased in 5 mM Tris−EDTA, while ^{3}H-labeled protofibrils were produced efficiently in 50 mM Tris−EDTA containing 0−60 mM NaCl.

Soluble protofibrils recovered in the supernatants of aggregation reactions such as those in Figure 2 were separated from residual Aβ(1−40) monomer by SEC on Superdex 75. Clear separation was achieved between protofibrils, which eluted in the column void volume, and monomers (Figure 3), and profiles for radiolabeled and unlabeled protofibril preparations were similar (data not shown). Subsequent SEC analyses indicated that isolated radiolabeled protofibrils in 50 mM Tris−EDTA or unlabeled protofibrils in 5 mM Tris−EDTA slowly generated monomer with a half-life of ≫5 h at room temperature. Figure 3 also demonstrates that radiolabeling of Aβ(1−40) permits protofibril concentrations to be determined more accurately. Protofibrils scatter significant amounts of light, causing the ratio of apparent absorbance at 280 nm to radiolabel to be about 3-fold higher in the protofibril peak than in the monomer peak. Therefore, unlabeled protofibril concentrations estimated only by absorbance at 280 nm were corrected by factors of 2.2−3.5, a value that depended largely on the size of the protofibrils.

Size Analysis of Aβ Protofibrils by Light Scattering. The size and yield of Aβ protofibrils were dependent on several features of the aggregation reaction including ionic strength, pH, and monomeric Aβ concentration. DLS was a convenient technique for size comparisons between protofibril preparations, and careful control of the aggregation conditions resulted in reproducible protofibril pools. Values of R_H for pooled Aβ protofibrils eluted from Superdex 75 ranged from 46 to 64 nm for unlabeled and from 24 to 51 nm for radiomethylated Aβ protofibrils.

To obtain information about protofibril molecular masses, we employed a DAWN EOS multi-angle light scattering (MALS) instrument in-line with SEC. MALS uses an array of detectors at fixed angles to measure the intensity of scattered light. Extrapolation of the angular dependence of the light scattering signal to 0° provides an estimate of the sample molecular mass (M_w), which requires that the sample concentration be known, and the root-mean-square radius (R_{gz}), which is independent of concentration (*49*) (see eqs 1 and 2). MALS is attractive because, in contrast to DLS, M_w estimates can be made without assumptions of protofibril shape. MALS analysis was conducted on protofibrils as they eluted in the void volume on Superdex 75 as in Figure 3. For onput protofibrils with an average R_H of 50 nm by DLS, the Zimm plot in Figure 4 gave a $M_w = 18 \times 10^3$ kDa and an R_{gz} of 65 nm. With other protofibril preparations, M_w values ranged from 7×10^3 to 32×10^3 kDa and R_{gz}, from 50 to 120 nm. The large size of Aβ protofibrils resulted in only slight size separation by SEC on Superdex 75. M_w and R_{gz} values decreased by up to a factor of 2 from the leading edge to the trailing edge of the intervals analyzed in Figure 4, although their ratio (proportional to M_w/L_z in Table 1 below) decreased by less than 20% over this range. In addition, the largest protofibrils appeared to be filtered out, as R_H values decreased by 0−30% in the eluted pool relative to the onput (see Table 1 below). Because of protofibril polydispersity in the eluted fractions, it was important to use the same protofibril preparation to compare the protofibril elongation and association reactions described below.

Mechanisms of Aβ Protofibril Growth. While studies of Aβ fibril formation have examined Aβ monomer aggregation (*14*) and Aβ fibril extension by monomer deposition (*26*, *33*, *53*), few reports have focused on protofibril growth in solution. Since mature Aβ fibrils have a greater length and diameter than Aβ protofibrils, several possible mechanisms of protofibril growth may exist. We have distinguished two growth processes: protofibril extension by monomer deposition, a process we term elongation, and direct protofibril−protofibril association. The rates of both growth processes were essentially unaffected by the presence of 5 μM thioflavin T in the reaction medium (data not shown). Elongation could be conveniently followed by the fluorescence increase following addition of purified Aβ monomer to purified protofibrils. This is illustrated in Figure 5A, where addition of 30 μM Aβ(1−40) monomer resulted in a rapid increase in fluorescence from about 60 to 280 units over 40 min. Parallel measurements of the average R_H showed an

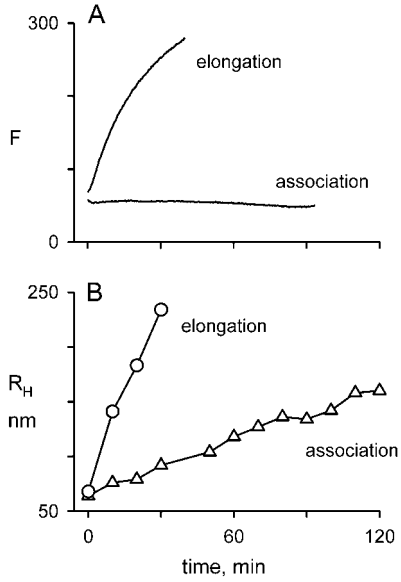

FIGURE 5: Protofibril growth arises from direct protofibril association and from elongation by added monomer. Both growth processes were studied with unlabeled Aβ(1−40) protofibrils isolated as in Figure 3 but with Superdex 75 equilibrated in 5 mM Tris−EDTA. The protofibril stock was diluted to a final concentration of 1.3 μM (in Aβ residue units) in 50 mM Tris−EDTA with the additions indicated below. Reactions were incubated at 25 °C without agitation in the fluorometer for continuous monitoring of thioflavin T fluorescence (F) (panel A) and in the DLS instrument for R_H determination at the indicated times (panel B). For elongation measurements, SEC-purified Aβ(1−40) monomer was added to 30 μM. For association measurements, NaCl was added to 150 mM. Incubations without addition of either monomer or NaCl showed no significant change in fluorescence or R_H over a 2 h period (data not shown).

increase from 68 to 234 nm during the same time course (Figure 5B). These data confirm that protofibrils grow in size immediately upon addition of monomer and that this growth corresponds to an extension of β-sheet structure as indicated by an increase in thioflavin T binding. Protofibril interactions in the absence of added Aβ monomer have been observed previously by DLS (*17*) and AFM (*28*). We observed in preliminary experiments that protofibril association was very sensitive to ionic strength and occurred at a very slow rate if at all in the absence of NaCl. This effect of NaCl on protofibril association appears to be related to the NaCl effect on Aβ aggregation in Figure 2, a point that we consider further under Discussion. Following addition of 150 mM NaCl to the initial protofibrils in Figure 5, the average protofibril R_H increased from 64 to 160 nm over 2 h (Figure 5B). Thioflavin T fluorescence during this 2 h period showed little change (Figure 5A), indicating that β-sheet structure was retained and that little dissociation occurred during the incubation.

To support our interpretation that the observed R_H increases without added Aβ monomer in Figure 5 reflected protofibril association, we took care to remove any initial monomeric Aβ from the protofibril pool immediately prior to the association reaction. However, the protofibril pool was polydisperse, and it was important to rule out any possibility that monomer could dissociate from smaller protofibrils and then rapidly re-deposit onto larger protofibrils. We conducted double isotope labeling experiments to address this question. A fresh preparation of [^{3}H]Aβ protofibrils was incubated with 150 mM NaCl and 1 μM [^{14}C]Aβ(1−40) monomer under

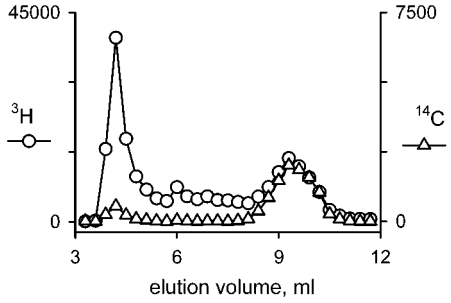

FIGURE 6: Protofibril growth in the absence of added monomer does not involve a monomer dissociation/re-deposition process. [^{3}H]Aβ(1−40) protofibrils (1.5 μM) isolated as in Figure 3 were incubated with [^{14}C]Aβ(1−40) monomer (1 μM) in 50 mM Tris−EDTA and 150 mM NaCl for 20 h prior to separation on Sepharose CL-2B as outlined under Experimental Procedures. Fractions were collected, and radioactivity (DPM) was measured by scintillation counting: ^{3}H (circles) and ^{14}C (triangles). DPM were converted to pmol of Aβ(1−40), and molar ratios were determined in each fraction. Recovery of radioactivity in eluted fractions was >90% of the onput.

the conditions outlined in Figure 5. This concentration of ^{14}C-labeled monomer far exceeds the level of ^{3}H-labeled monomer observed after incubation of 1−2 μM [^{3}H]-protofibrils alone. The protofibril R_H increased from 51 to 143 nm over 20 h. Following centrifugation and SEC of the reaction mixture, ^{14}C and ^{3}H radioactivity in each fraction was determined by scintillation counting. A process of dissociation and re-deposition would create a transient pool of mixed ^{3}H- and ^{14}C-labeled monomer and result in significant incorporation of ^{14}C into the growing [^{3}H]Aβ protofibril. However, the ^{14}C/^{3}H molar ratio reached only 0.06 in the protofibril peak (Figure 6). Since our general observations indicate that percentage increases in R_H (by DLS) and M_w (by MALS) during protofibril association reactions are nearly proportional, the R_H increase in this experiment would predict a nearly 3-fold increase in M_w. Such an increase cannot be explained by the small amount of ^{14}C incorporation, and we conclude that the increase in protofibril size during association reactions does not involve significant monomer deposition. Monomer deposition does occur at a very slow rate at low monomer concentration and probably accounts for the small amount of [^{14}C]monomer incorporated into the [^{3}H]protofibrils.

To characterize the protofibril growth products generated in Figure 5 more thoroughly, the elongated protofibrils, the associated protofibrils, and the initial protofibril pool were analyzed by SEC-MALS. Samples were loaded on Superdex 75 as in Figure 3, and the elution was monitored in-line by UV absorbance and MALS. A similar series of elongation and association experiments carried out on radiomethylated Aβ protofibrils also was analyzed by SEC-MALS. Recoveries of the elongated and associated protofibrils from the SEC column were lower than those of the initial protofibrils, suggesting that growth prevented some of the larger protofibrils from passing through the column. DLS measurements confirmed this loss, as R_H values of the recovered elongated and associated protofibrils were considerably lower than those of the onput samples (Table 1). Nevertheless, the results in Table 1 show very similar trends for the labeled and unlabeled protofibril growth products. Zimm plots were used to obtain M_w and R_{gz} values. Relative to the initial protofibrils, estimated M_w values increased by factors of 3−6 for the

Table 1: Comparison of SEC-MALS Parameters for Elongated and Associated Protofibrils[a]

	pre-SEC R_H (nm)	post-SEC R_H (nm)	R_{gz} (nm)	M_w (kDa)	M_w/L_z	M_L (kDa/nm)
unlabeled Aβ(1−40)						
initial protofibril	64	51	100	30×10^3	88	nd
elongated protofibril	221	143	225	57×10^3	73	63
associated protofibril	169	104	162	86×10^3	157	150
radiolabeled Aβ(1−40)						
initial protofibril	47	nd	121	19×10^3	48	nd
elongated protofibril	93	75	187	24×10^3	38	46
associated protofibril	195	112	203	76×10^3	110	109

[a] Samples (0.5 mL, 1−2 μM protofibril) from the protofibril pool and from elongation and association reactions similar to those in Figure 5 were applied to Superdex 75 equilibrated in 5 mM Tris−EDTA and in-line with a DAWN EOS MALS unit (see Experimental Procedures). Some 30−40 intervals across the protofibril peak were analyzed as in Figure 4 to obtain values of M_w, R_{gz}, and M_w/L_z and with eq 8 to obtain M_L. Parallel experiments were conducted on control, elongated, and associated ^{3}H-radiomethylated Aβ(1−40) protofibrils eluted from Superdex 75 in 50 mM Tris−EDTA. Additional experiments with unlabeled protofibrils ($n = 4-6$) gave M_w/L_z of 95 ± 22 (SD), 87 ± 12, and 257 ± 71 kDa/nm for initial, elongated, and associated protofibrils, respectively. Additional experiments with radiolabeled protofibrils ($n = 3-5$) gave M_w/L_z of 85 ± 52, 61 ± 30, and 201 ± 84 kDa/nm for initial, elongated, and associated protofibrils, respectively. The ratio of M_w/L_z to M_L in all cases was close to unity [1.06 ± 0.20 (SD), $n = 15$]. For reference, DLS measurements of R_H for protofibrils in onput (pre-SEC) and eluted pools (post-SEC) are included.

associated protofibrils but only about 1.3−2 for the elongated protofibrils. In contrast, roughly comparable 2-fold increases in R_{gz} were observed for both elongated and associated protofibrils. Fitting the angular dependence of the light scattering from selected intervals of the SEC-MALS runs to eq 4 revealed that all three protofibril samples corresponded closely to rigid rods. Converting the R_{gz} values to L_z for rigid rods allowed estimates of the mass per unit length M_w/L_z (Table 1). Some variation in M_w/L_z was observed within each class of protofibrils. Nevertheless, the M_w/L_z for associated protofibrils was consistently higher than that for elongated protofibrils in paired experiments by a factor of 3.1 ± 0.7 (SD, $n = 7$). To investigate whether polydispersity could affect these M_w/L_z estimates, selected intervals were again analyzed with eqs 6 and 7, which incorporate an explicit M_w distribution function. This analysis moved the protofibril shapes slightly in the direction of semiflexible chains (e.g., l_k decreased from >50 000 to 1400 nm for the elongated labeled protofibrils) but had no effect on M_w/L_z. As a further check on any possible distortion of the data by polydispersity, the analysis was repeated with the Casassa plots in eq 8. This plot, whose application is limited to large values of qL, offers the advantage that the weight average mass per unit length M_L is obtained independently of the distribution of molecular lengths in the sample. Thus, if the protofibril cross-sectional areas are relatively uniform in each sample, M_L provides a good estimate of the mass per unit length. Values of qL for both the elongated and the associated protofibrils fell within the range in which the Casassa plots were predicted to be linear (Figure 7), and the M_L estimates obtained were in good agreement with the previous values of M_w/L_z (Table 1). Values of qL for the initial protofibril pools did not fall in this range (Figure 7), preventing M_L estimates for these samples.

Murphy and colleagues have previously shown that MALS is useful in probing mechanisms of Aβ aggregation (*16*, *41*). They calculated M_w/L_z values ranging from 4 to 60 kDa/nm for Aβ(1−40) aggregated for several hours in PBS (*54*). Given uncertainties in determining concentrations of the aggregates in the absence of a radiolabel, these estimates are in reasonable agreement with the range of M_w/L and M_L estimated for elongated protofibrils from our SEC-MALS data (40−100 kDa/nm).

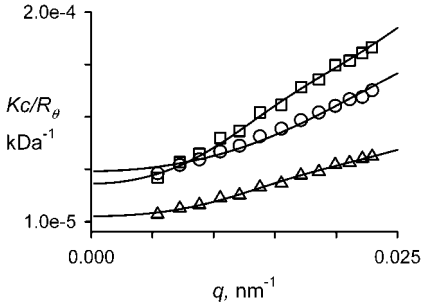

FIGURE 7: Analysis of MALS from elongated and associated protofibrils as suggested by Casassa (*46*) (eq 8). A typical interval of data from each of the three radiolabeled protofibril samples analyzed in Table 1 was plotted according to eq 8 to assess the range of qL over which the plots become linear. Each of the three data sets was also analyzed with the semiflexible chain model (eq 4 and the reciprocal of eq 6 with $N = 1$), and the fitted curve was graphed according to eq 8 to give the lines shown. Both the points and the lines for the elongated (□) and the associated (△) protofibrils were linear over most of the range of measurements, allowing calculation of M_L, but the line for the initial protofibril pool (○) did not reach a linear range and ruled out an M_L determination.

The large increase in M_w for associated protofibrils also resulted in a greater proportion of sedimenting fibrils compared to elongated protofibrils. The R_H for associated unlabeled Aβ protofibrils in Table 1 progressed from 64 to 281 nm after 40 min prior to SEC-MALS. Centrifugation of the solution sedimented 60% of the light scattering intensity by DLS and reduced the R_H to 169 nm. The R_H for elongated protofibrils increased from 64 to 197 nm after 25 min, and sedimenting fibrils were not detected by loss of light scattering intensity.

Visualization of Elongated and Associated Protofibrils by AFM and EM. AFM has previously revealed periodicity and branching in air-dried samples of Aβ fibrils (*20*, *55*). AFM analysis of Aβ(1−40) protofibrils generated in PBS found spherical species and wormlike structures 20−600 nm in length. The diameters of these particles, estimated from heights in topography scans of air-dried samples, were 3−4 nm (*28*, *56*). AFM analysis of our protofibril samples showed striking changes after elongation and association. The initial protofibril pool consisted of small aggregates with a globular appearance, rigid rods (<1 μm length), and globular ag-

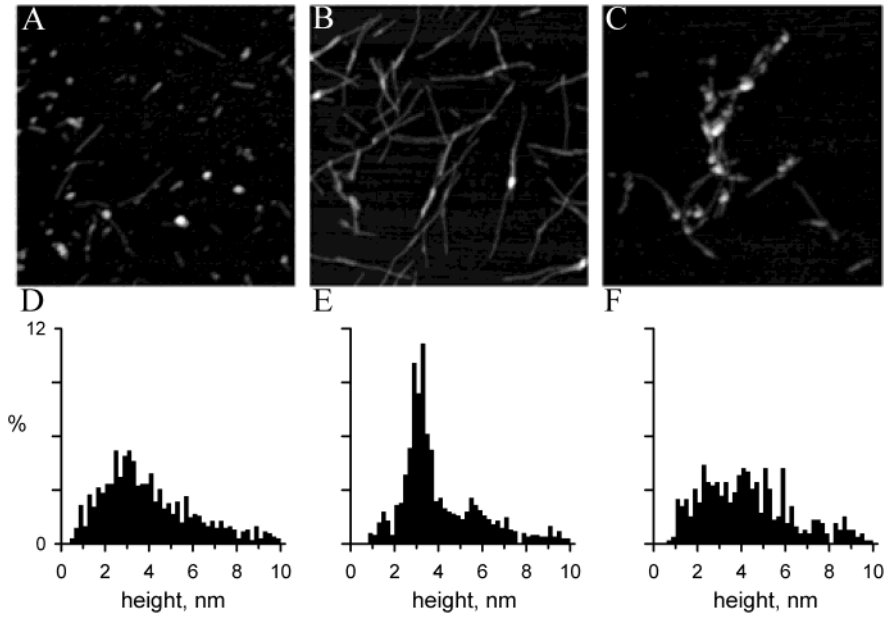

FIGURE 8: Protofibril growth monitored by AFM. Initial (panels A and D), elongated (panels B and E), and associated (panels C and F) protofibrils (100 μL) from the unlabeled samples in Table 1 were applied to mica stubs and analyzed by AFM as outlined under Experimental Procedures. Panels A−C: 2 μm × 2 μm insets of 5 μm × 5 μm images. Panels D−F: Height distributions of all particles >0.5 nm observed on multiple horizontal and vertical lines through these images are shown as histograms. These distributions tabulate the frequency of particle heights in 0.2 nm increments and represent 500−1000 measurements in each image. The initial and elongated protofibril samples were taken from the SEC void volume peaks, but low recovery of associated protofibrils after SEC required that this sample be taken from the SEC onput.

gregates with rods emanating from them (Figure 8A). After elongation, the proportion of aggregates corresponding to rods increased, and these rods were longer (Figure 8B). Elongated protofibrils analyzed by AFM prior to SEC included long wispy tendrils extending to lengths of several micrometers (data not shown). Length measurements of the elongated protofibrils in Figure 8B gave a distribution in general agreement with the L_z of 780 nm from Table 1. In contrast, protofibril association induced by added NaCl resulted in clustering of the initial protofibrils and no extension of tendrils (Figure 8C). Negatively stained EM images of elongated or associated protofibrils reinforced these observations. Elongation gave filamentous or ribbonlike protofibrils (Figure 9C), while association resulted in less-ordered clustering of protofibril segments generally in a staggered fashion along their lateral surfaces rather than at their ends (Figure 9B). AFM showed a rather broad range of particle heights in the initial protofibril pool, as demonstrated by the height distribution plot in Figure 8D with a peak at about 3 nm. After protofibril elongation, the height distribution became narrower and enriched at a peak of 3.1 nm (Figure 8E). Virtually all of the 3.1 nm heights in Figure 8B corresponded to rodlike filaments, and many structures with heights greater than 4 nm appeared to be bundles of filaments. The height distribution of the associated protofibrils in Figure 8F was similar to that of the initial protofibrils. The height of large clusters such as that in Figure 8C generally exceeded 5 nm throughout, causing a slight shift in the associated protofibril distribution to larger heights.

To obtain further information about the effects of NaCl on protofibril growth, we compared protofibrils elongated with and without 150 mM NaCl for 19 h. Filamentous or ribbonlike structures composed of both single and multiple longitudinal strands were seen in both samples (Figure 9C, D), but the pattern of negative staining differed. Individual strands within the elongated protofibrils were more pronounced in the sample elongated with NaCl (Figure 9D), and the widths of the strands in these protofibrils were slightly larger than the widths of those elongated in the absence of salt (Figure 9C). Further experiments will be necessary to determine whether these strand width differences result from the inclusion of NaCl during elongation or whether they arise from more random patterns of negative stain uptake from sample to sample.

Elongation Rates after Protofibril Growth. We hypothesize that Aβ(1−40) monomer deposition occurs at the ends of the small protofibrils we isolate after aggregation at low ionic strength. This elongation hypothesis is supported by several observations. The AFM analysis in Figure 8 shows that elongated protofibrils have the same diameter but considerably longer lengths than the initial protofibrils, and the SEC-MALS analysis in Table 1 is consistent with growth in a longitudinal rather than a lateral direction. Furthermore, rates of elongation at a fixed monomer concentration are proportional to the protofibril concentrations as dilutions are made from a common protofibril stock (data not shown). If it is thus assumed that elongation rates are proportional to the concentration of protofibril ends, then comparison of elongation rates following protofibril growth by elongation or association provides information about the structural processes occurring during growth. In particular, if the number concentration of initial protofibrils is maintained during growth, the relative elongation rates will indicate whether ends have been lost by sequestration or capping or in fact created.

An isolated Aβ(1−40) protofibril stock (R_H = 70 nm) was incubated at 5 μM for 2 h with either 15 μM Aβ monomer (to induce elongation) or 150 mM NaCl (to promote association) under conditions otherwise identical to those in Figure 5. A 2-fold increase in both R_H and thioflavin T fluorescence was observed in the protofibril elongation

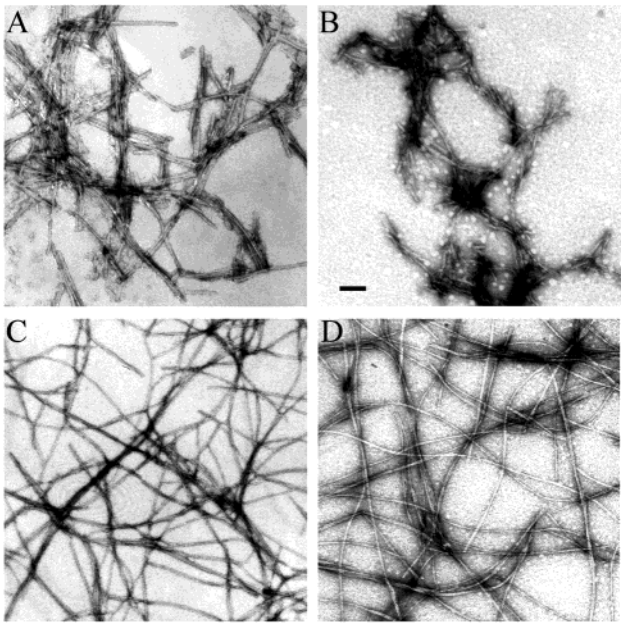

FIGURE 9: Electron micrographs of radiomethylated Aβ(1−40) fibrils and protofibrils. Panel A: [^{3}H]Aβ(1−40) fibrils were prepared as in Figure 2 with buffer containing 150 mM NaCl. At 144 h, fibrils were sedimented by centrifugation at 18000*g*. The supernatant was removed, and the pellet was washed and gently suspended in water and applied to a grid without dilution. Grids were analyzed by EM as described under Experimental Procedures. Panel B: Labeled protofibrils were associated as in Figure 5 for 19 h, and an aliquot was prepared for EM. Panels C and D: Labeled protofibrils were elongated with 40 μM SEC-purified monomer as in Figure 5 in the absence (panel C) or presence (panel D) of 150 mM NaCl for 19 h, and aliquots were prepared for EM. Elongated protofibrils consisted of both single- and multiple-stranded filaments or ribbons. Average widths of the single strands, measured as outlined under Experimental Procedures, were 5.9 ± 0.9 nm (SD, $n = 59$) in panel C and 8.3 ± 1.7 nm ($n = 65$) in panel D. Images are shown relative to a calibration bar of 0.1 μm.

reaction, while the associated protofibrils increased in R_H by almost 4-fold with little change in thioflavin T fluorescence. Dilutions of the elongated and associated protofibril reactions and of the initial protofibril pool to an equal number concentration of original protofibrils were then made into solutions containing 35 μM Aβ(1−40) monomer and 5 μM thioflavin T, and the fluorescence was monitored continuously as shown in Figure 10. The new elongation rates were nearly identical for all three protofibril preparations. The elongation rate data support the conclusion that the initial number of protofibril ends was retained without change during both the elongation and association reactions.

DISCUSSION

Our current study revealed several features of Aβ aggregation that have not been appreciated previously. After the following brief summary of these features, we compare our observations with previous biophysical studies of in vitro Aβ aggregation in subsequent sections. We found that the lag time for in vitro Aβ(1−40) aggregation was increased at NaCl concentrations below the physiological concentration, and the yield of protofibrils was about an order of magnitude higher at low ionic strength. Radiolabeling by reductive methylation of primary amine groups at the N-terminus and Lys16 and Lys28 slowed the rate of Aβ(1−40) aggregation but had little effect on protofibril structure.

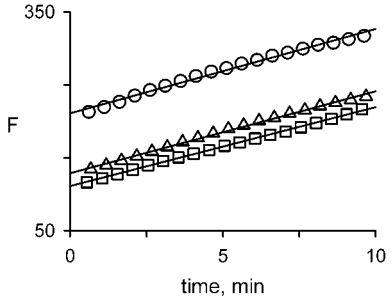

FIGURE 10: Comparison of monomer deposition rates for elongated and associated protofibrils. Unlabeled Aβ(1−40) protofibrils isolated by SEC in 5 mM Tris−EDTA as in Figure 3 were incubated at 5 μM with 15 μM monomer without NaCl for elongation, at 2.5 μM in 150 mM NaCl without monomer for association, or at 5 μM without monomer or NaCl as a control. Following a 2 h incubation without agitation, samples were diluted into 50 mM Tris−EDTA, 150 mM NaCl, 5 μM ThT, and 35 μM Aβ(1−40) monomer to a final concentration corresponding to 1 μM initial protofibril. Rates of elongation were then obtained by linear regression analysis of the thioflavin T fluorescence (*F*) with time for elongated protofibrils (circles), associated protofibrils (squares), and the initial protofibril pool (triangles) and corresponded to 11.6, 10.8, and 11.3 *F*/min, respectively.

Radiolabeling also permitted more accurate MALS determinations of the M_w and mass per unit length of the protofibrils, because protofibril concentrations were determined by absorbance calibrated with radiolabel rather than by absorbance alone. A clear distinction was made between protofibril growth by elongation with monomer in the absence of NaCl and growth by protofibril association with NaCl in the absence of monomer, as the mass per unit length of the associated protofibrils was 2−3 times that of the elongated protofibrils. The data from MALS were integrated with images from AFM to clarify and confirm this structural difference. Protofibril elongation resulted from monomer deposition only at the ends of protofibrils and proceeded without an increase in protofibril diameter. In contrast, protofibril association involved lateral associations that resulted in a relatively disordered fibril structure. Finally, protofibril growth by elongation or association did not result in any capping or other reduction of protofibril ends available for elongation with monomer.

Early models of nucleation-dependent Aβ polymerization (*14*, *57*) did not specify the pathways by which nuclei grow to become fibrils. The incorporation of protofibrils as intermediates in the growth process still did not establish the mechanisms of protofibril growth (*15*, *28*). However, even before the identification of protofibrils, the growth of Aβ aggregates by monomer deposition and direct aggregate interaction had been proposed (*26*, *33*, *51*, *58*). The smallest Aβ(1−40) aggregates isolated by SEC and analyzed by DLS typically show average R_H values in the range of 20 nm (*15*), and the R_H values continuously increase to >100 nm during incubation of the aggregates at physiological ionic strength in the presence of monomeric Aβ (*17*, *59*). When growing protofibrils reach a mean R_H of about 250 nm, we observed some sedimentation at 18000*g*, thus defining the transition to fibrils. Aβ aggregates are classified as protofibrils not only by size but also by their binding of thioflavin T, their high content of β structure by circular dichroism (*17*), and their morphology in EM and AFM (*17*, *22*, *56*). Our ratios of thioflavin T fluorescence to Aβ(1−40) concentration are the same for radiomethylated protofibrils and fibrils, suggesting

that this fluorophore binds to similar secondary structures in both aggregates. A similar previous observation was based on thioflavin T binding to unlabeled Aβ(1−40) protofibrils and fibrils (*17*).

Protofibril size and morphology may be determined in part by the method of preparation. In two studies in which Aβ(1−40) protofibrils were examined in detail by EM and AFM, the initial Aβ stocks were dissolved in DMSO, diluted into PBS, and incubated without continuous agitation (*22, 56*). Under these conditions, pseudo-spherical aggregates (4 nm by AFM, 10 nm by EM) and short protofibrils (<50 nm in length) were seen within a few hours. Prolonged storage of Aβ(1−40) in DMSO prior to dilution and immediate examination resulted in much larger pseudo-spherical structures (*22*). When we conducted our typical aggregation reactions of SEC-purified Aβ(1−40) in NaCl without agitation, lag times of several days were observed. Furthermore, there was no significant accumulation of aggregates with R_H values less than 100 nm, even in the absence of NaCl (data not shown). We instituted vigorous agitation of the aggregation reactions to obtain the smaller Aβ(1−40) protofibrils that we describe here. Following Superdex 75 purification, these initial protofibril preparations had R_H values from 24 to 64 nm, and it was clear that the size was dependent on aggregation conditions and modifications to the peptide. Unlabeled Aβ(1−40) monomer formed larger protofibrils on a more rapid time scale than radiomethylated Aβ(1−40), and decreasing NaCl (150 mM to 0 mM) and Tris buffer concentrations (50 mM to 5 mM) resulted in smaller protofibrils. However, even the smallest protofibrils we observed were quite large. The smallest characterized by SEC-MALS gave a M_w of 7×10^3 kDa corresponding to about 1600 monomer units.

When we observed a pronounced dependence of fibril formation on salt concentration (Figure 2), we explored whether manipulation of ionic strength would allow us to distinguish protofibril growth by elongation from growth by association. An effect of NaCl in promoting Aβ aggregation had been observed previously. The solubility of Aβ(1−43) in water was substantially decreased by addition of buffered NaCl (*60*). Aβ(1−28) showed a remarkably greater rate of aggregation in physiological NaCl concentration than in 10 mM phosphate buffer (*58*), as monitored by DLS. The appearance of protofibrils by AFM and their growth rates were accelerated significantly when NaCl was added to monomeric Aβ(1−40) in 100 mM phosphate buffer (*28*). However, our study appears to be the first in which small Aβ(1−40) protofibrils were isolated free of residual monomer and directed along either elongation or association pathways by adjustment of the monomer and NaCl concentrations. Elongation rates were slowed somewhat at lower salt concentrations, but association reactions were virtually stopped. One possible way in which NaCl could promote association is by increasing protofibril diameters. These diameters are determined by at least three levels of structural features (*61, 62*). Fully extended peptide segments align to form β-sheets with the peptide strands perpendicular to and inter-strand H-bonds parallel to the fibril axis. Individual filaments, sometimes called protofilaments, are composed of laminates of these sheets which twist about the filament axis. The diameter of the filament, therefore, is determined by the length of the aligned peptide segments and the number of laminated sheets, with four to six sheets typically proposed (*61, 63*). Fibrils are composed of associated filaments. Cross-sectional analyses of electron microscope images of amyloid fibrils formed by a number of proteins (*62*) as well as Aβ(6−25) (*23*) show four to six close-packed filaments running parallel to the fiber axis (*62*). NaCl thus could increase fibril diameters by inducing a greater number of laminated sheets in the filament or by stabilizing close packing of more filaments in the fibril. Moreover, NaCl could promote lateral interaction of fibrils themselves.

A strong indication that the products of protofibril elongation and association differ was obtained from size analysis by SEC-MALS. M_w/L_z values, denoting protofibril mass per unit length, decreased during elongation and increased during association reactions. The ratio of M_w/L_z for associated protofibrils to M_w/L_z for elongated protofibrils was about 3 (see Results). From these SEC-MALS data alone, we might be tempted to propose that protofibrils correspond to a single helical β-sheet filament and that 150 mM NaCl promotes lateral association of protofibrils into fibrils that contain several parallel filaments. However, the entirety of our SEC-MALS data does not support this proposal. M_w/L_z for both initial protofibrils and elongated protofibrils varied among preparations. The smallest M_w/L_z values were observed after elongation of initial protofibrils that showed the lowest R_H values by DLS. It is unlikely that the mass per length of a single filament protofibril would vary as much as suggested by the range of M_w/L_z values, and AFM data confirmed that the initial protofibrils were more diverse than single filament structures. AFM analysis of our SEC-purified protofibril stocks revealed a mixture of small globular aggregates, rigid rods (<1 μm length), and globular aggregates with protruding rods (Figure 8A). Graphical analysis of the particle height distribution emphasized this heterogeneity (Figure 8D).[2] Elongation increased the percentage of rigid rods (Figure 8B) and slightly enriched the proportion of structures with a height centered at 3.1 nm (Figure 8E). However, even the elongated protofibrils still exhibited height heterogeneity by AFM, indicating that the lowest M_w/L_z values of 73 kDa/nm for unlabeled and 38 kDa/nm for labeled elongated protofibrils (Table 1) are higher than the true M_w/L_z of the 3.1 nm protofibrils. If the height distribution is assumed to reflect the actual distribution of M_L and M_w/L_z of the elongated protofibrils in solution, an M_i/L_i for the 3.1 nm protofibrils can be determined from eqs 9 and 10. From the height distribution for the elongated protofibrils in Figure 8E, we calculated an $\langle h^2 \rangle_w$ of 38.2 nm^2. Combining this value with an $M_L \cong M_w/L_z$ of 73 kDa/nm, an M_i/L_i of 18 kDa/nm was calculated for the 3.1 nm particles from eq 10. A somewhat larger M_i/L_i would be calculated if the higher particles in Figure 8E were assumed to form only on the mica surface and were rejected. These data are in reasonable agreement with STEM studies by Goldsbury et al. of amyloid protofibrils and fibrils formed by Aβ(1−40) (*22*) and amylin(1−37) (*66*). After calibration with a particle of known density like tobacco mosaic virus, STEM provides quantitative estimates of the mass-per-length (MPL) of a filament or fibril. An MPL value of 19 ± 2 kDa/nm was obtained for Aβ(1−40)

[2] AFM measurements of protofibril heights in air-dried samples may differ from those obtained with the same protofibrils in solution (*64, 65*), and our height distribution analysis should be interpreted as indicating only relative heights.

protofibrils, whereas distributions were observed for fibrils that were resolved into discrete MPLs of 21, 31, and 42 for Aβ(1−40) and 22, 30, 41, and 51 for amylin. Detailed fibril height distributions from AFM have not been reported for Aβ(1−40) previously, but up to three populations corresponding to 2−3, 4−6, and 8−12 nm have been noted (*55*, *56*). Therefore, it is plausible that the 3.1 nm protofibrils that we observe by AFM correspond to the 19 kDa/nm protofibrils reported by Goldsbury et al. As these authors point out, an MPL of 19 kDa/nm is consistent with a model (*67*) in which 48 Aβ monomers, each with an antiparallel β-sheet hairpin, form four laminated sheets and extend for one helical turn of β-sheet of length 11 nm.

The increase in M_w/L_z and M_L obtained from SEC-MALS following protofibril association suggested a lateral association, induced by the introduction of a physiological NaCl concentration, that increased the diameter of the associated protofibrils. However, the SEC-MALS data did not indicate the extent to which the lateral alignment was ordered. Both our AFM and EM images (Figures 8C and 9B) indicated that the alignment was not well ordered and that aggregates consisting of clumps of the short initial protofibrils were generated. These bundled aggregates bore some resemblance to Aβ(1−40) fibrils formed in one report at pH 5.8 (*36*) and in another at pH 7.4 following vigorous agitation (*22*). Our radiomethylated Aβ(1−40) fibrils obtained after aggregation for 144 h with agitation (Figure 9A) also appear similar to the associated protofibrils. Thus, it seems clear that 150 mM NaCl promotes lateral association of Aβ(1−40) fibrils, but it is less clear whether NaCl alters the structure of the fibril itself. When more ordered fibrils generated by elongation with monomer in the presence and absence of 150 mM NaCl over 20−60 h periods were compared, wider strands were measured by EM in the presence of NaCl (see Figure 9C, D). Whether this observation reflects differences in the number of filaments or laminated sheets in the fibrils remains to be determined.

An important conclusion in our studies was that neither protofibril elongation nor association caps protofibrils or otherwise decreases the number of ends available for elongation. This feature was confirmed when we compared the monomer deposition rates of elongated protofibrils and associated protofibrils with that of the initial protofibril pool. All three deposition rates were the same (Figure 10). Elongation by monomer deposition at protofibril ends is consistent with previous conclusions about monomer addition to Aβ fibrils (*26*, *33*, *53*). Rate constants for addition in these studies were first order in both fibril and monomer concentrations. We also have observed elongation rate constants that are first order in both protofibril and monomer concentration, although some experiments revealed a second-order dependence on monomer concentration (data not shown). The conditions necessary to reproducibly demonstrate this second-order dependence have not yet been identified. Our proposal that protofibrils associate without a loss of ends available for monomer deposition may differ slightly from previous, less specific suggestions that protofibrils associate by an end-to-end mechanism (*28*, *54*). For example, AFM studies of Aβ(1−40) aggregation observed that the initial appearance of protofibrils was followed by a decrease in overall protofibril number and an increase in protofibril length. End-to-end protofibril coalescence was proposed to explain the time-dependent elongation, since the protofibrils did not increase in height (*28*). However, other interpretations of these data are possible. For example, the decrease in protofibril number may be due to adsorption loss (we find that protofibrils are progressively adsorbed to vessel walls, especially at physiological ionic strength), and the length increase then can be attributed to continued monomer deposition.

While we are as yet unable to directly monitor reactions leading to the formation of nuclei and their transition to protofibrils, we can make some inferences about these reactions because they are thought to be rate limiting in the initial aggregation of Aβ monomers. In buffers at physiological ionic strength, growth by elongation and association is likely to occur simultaneously, and such growth may lead to a structure with more lateral order than we see following association of protofibrils in the absence of monomer in Figure 9B. The lag time for aggregate formation was decreased by a physiological NaCl concentration (Figure 2), the same condition that promotes protofibril association, suggesting that the formation of nuclei or their growth involves association reactions of the same Aβ peptide surfaces involved in protofibril association. Radiomethylation of Aβ(1−40) increased the lag time for aggregate formation, and rates of both elongation and association of the radiomethylated protofibrils were slower than those of unlabeled protofibrils. The decreased reactivity of radiomethylated Aβ(1−40) may arise from unfavorable steric interactions caused by the addition of two methyl groups on Lys16 and Lys28. A recent report indicates that Lys28 is partially inaccessible to radiomethylation in Aβ(1−40) fibrils (*68*), and Lys16 is located near the Aβ peptide central hydrophobic region believed to be important for self-assembly (*69*). Methylation of these Lys residues thus may be viewed as analogous to site-specific mutations that alter the ability of Aβ(1−40) to aggregate (e.g., *15*, *70*, *71*). Identification of the surfaces involved in protofibril elongation and association may reveal distinct hydrophobic and electrostatic interactions that can be targeted by inhibitors. For example, inhibitors that cap protofibril ends by specific high-affinity binding would inhibit elongation at low, substoichiometric concentrations. Compounds that disrupt lateral association also may be effective inhibitors of fibril formation. To cite one related observation, Lynn and co-workers were able to prevent the lateral association of Aβ(10−35) filaments into full-width fibrils by C-terminal modification of this Aβ peptide with (poly)ethylene glycol (*72*).

ACKNOWLEDGMENT

We are grateful to Amanda Singleton (Mayo Clinic) and Ganesh Kamath (Mayo Clinic) for technical assistance in the early phases of this work, to Dr. Michael McKinney (Mayo Clinic) for the use and guidance of the AIS software, and to Ahmed Fadl (Johns Hopkins University School of Medicine) for assistance with AFM imaging.

REFERENCES

1. Cohen, A. S., and Calkins, E. (1959) *Nature 183*, 1202−1203.
2. Terry, R. D., Gonatas, N. K., and Weiss, M. (1964) *Am. J. Pathol. 44*, 269−297.
3. Terry, R. D. (1985) *Textbook of Neuropathology*, Williams & Wilkins, Baltimore, MD.
4. Glenner, G. G., and Wong, C. W. (1984) *Biochem. Biophys. Res. Commun. 120*, 885−890.

5. Miller, D. L., Papayannopoulos, I. A., Styles, J., Bobin, S. A., Lin, Y. Y., Biemann, K., and Iqbal, K. (1993) *Arch. Biochem. Biophys. 301*, 41−52.
6. Kang, J., Lemaire, H.-G., Unterbeck, A., Salbaum, J. M., Masters, C. L., Grzeschik, K.-H., Multhaup, G., Beyreuther, K., and Muller-Hill, B. (1987) *Nature 325*, 733−736.
7. Goldgaber, D., Lerman, M. I., McBride, O. W., Saffiotti, U., and Gajdusek, D. C. (1987) *Science 235*, 877−880.
8. Tanzi, R. E., Gusella, J. F., Watkins, P. C., Bruns, G. A., P., S. G.-H., Van Keuren, M. L., Patterson, D., Pagan, S., Kurnit, D. M., and Neve, R. L. (1987) *Science 235*, 880−884.
9. Robakis, N. K., Ramakrishna, N., Wolfe, G., and Wisniewski, H. M. (1987) *Proc. Natl. Acad. Sci. U.S.A. 84*, 4190−4194.
10. Duff, K., Eckman, C., Zehr, C., Yu, X., Prada, C. M., Perez-tur, J., Hutton, M., Buee, L., Harigaya, Y., Yager, D., Morgan, D., Gordon, M. N., Holcomb, L., Refolo, L., Zenk, B., Hardy, J., and Younkin, S. (1996) *Nature 383*, 710−713.
11. Hsiao, K., Chapman, P., Nilsen, S., Eckman, C., Harigaya, Y., Younkin, S., Yang, F., and Cole, G. (1996) *Science 274*, 99−102.
12. Kawarabayashi, T., Younkin, L. H., Saido, T. C., Shoji, M., Ashe, K. H., and Younkin, S. G. (2001) *J. Neurosci. 21*, 372−381.
13. Yankner, B. A. (1996) *Nat. Med.* 850−852.
14. Jarrett, J. T., Berger, E. P., and Lansbury, P. T., Jr. (1993) *Biochemistry 32*, 4693−4697.
15. Walsh, D. M., Lomakin, A., Benedek, G. B., Condron, M. M., and Teplow, D. B. (1997) *J. Biol. Chem. 272*, 22364−22372.
16. Tomski, S. J., and Murphy, R. M. (1992) *Arch. Biochem. Biophys. 294*, 630−638.
17. Walsh, D. M., Hartley, D. M., Kusumoto, Y., Fezoui, Y., Condron, M. M., Lomakin, A., Benedek, G. B., Selkoe, D. J., and Teplow, D. B. (1999) *J. Biol. Chem. 274*, 25945−25952.
18. Yankner, B. A. (1996) *Neuron 16*, 921−932.
19. Pike, C. J., Burdick, D., Walencewicz, A. J., Glabe, C. G., and Cotman, C. W. (1993) *J. Neurosci. 13*, 1676−1687.
20. Harper, J. D., Lieber, C. M., and Lansbury, P. T., Jr. (1997) *Chem. Biol. 4*, 951−959.
21. Fezoui, Y., Hartley, D. M., Harper, J. D., Khurana, R., Walsh, D. M., Condron, M. M., Selkoe, D. J., Lansbury, P. T., Jr., Fink, A. L., and Teplow, D. B. (2000) *Amyloid 7*, 166−178.
22. Goldsbury, C. S., Wirtz, S., Muller, S. A., Sunderji, S., Wicki, P., Aebi, U., and Frey, P. (2000) *J. Struct. Biol. 130*, 217−231.
23. Fraser, P. E., Duffy, L. K., O'Malley, M. B., Nguyen, J., Inouye, H., and Kirschner, D. A. (1991) *J. Neurosci. Res. 28*, 474−485.
24. Malinchik, S. B., Inouye, H., Szumowski, K. E., and Kirschner, D. A. (1998) *Biophys. J. 74*, 537−545.
25. Teplow, D. B. (1998) *Amyloid 5*, 121−142.
26. Esler, W. P., Stimson, E. R., Ghilardi, J. R., Vinters, H. V., Lee, J. P., Mantyh, P. W., and Maggio, J. E. (1996) *Biochemistry 35*, 749−757.
27. Tseng, B. P., Esler, W. P., Clish, C. B., Stimson, E. R., Ghilardi, J. R., Vinters, H. V., Mantyh, P. W., Lee, J. P., and Maggio, J. E. (1999) *Biochemistry 38*, 10424−10431.
28. Harper, J. D., Wong, S. S., Lieber, C. M., and Lansbury, P. T., Jr. (1999) *Biochemistry 38*, 8972−8980.
29. Gill, S. C., and von Hippel, P. H. (1989) *Anal. Biochem. 182*, 319−326.
30. Means, G. E. (1977) *Method Enzymol. 47*, 469−478.
31. Haas, R., and Rosenberry, T. L. (1985) *Anal. Biochem. 148*, 154−162.
32. Levine, H. (1993) *Protein Sci. 2*, 404−410.
33. Naiki, H., and Nakakuki, K. (1996) *Lab. Invest. 74*, 374−383.
34. Jarrett, J. T., and Lansbury, P. T., Jr. (1992) *Biochemistry 31*, 12345−12352.
35. Evans, K. C., Berger, E. P., Cho, C. G., Weisgraber, K. H., and Lansbury, P. T., Jr. (1995) *Proc. Natl. Acad. Sci. U.S.A. 92*, 763−767.
36. Wood, S. J., Maleeff, B., Hart, T., and Wetzel, R. (1996) *J. Mol. Biol. 256*, 870−877.
37. Debye, P. (1947) *J. Phys. Colloid Chem. 51*, 18−32.
38. Zimm, B. H. (1948) *J. Chem. Phys. 16*, 1093−1099.
39. Neugebauer, T. (1943) *Ann. Phys. (Leipzig) 42*, 509−533.
40. Koyama, R. (1973) *J. Phys. Soc. Jpn. 34*, 1029−1038.
41. Shen, C. L., Fitzgerald, M. C., and Murphy, R. M. (1994) *Biophys. J. 67*, 1238−1246.
42. Zimm, B. H. (1948) *J. Chem. Phys. 16*, 1099−1116.
43. Flory, P. (1953) *Principles of Polymer Chemistry*, Cornell University Press, Ithaca, NY.
44. Bernocco, S., Ferri, F., Profumo, A., Cuniberti, C., and Rocco, M. (2000) *Biophys. J. 79*, 561−583.
45. Szegletes, T., Mallender, W. D., and Rosenberry, T. L. (1998) *Biochemistry 37*, 4206−4216.
46. Casassa, E. F. (1955) *J. Chem. Phys. 23*, 596−597.
47. Ferri, F., Greco, M., and Rocco, M. (2000) *Macromol. Symp. 162*, 23−43.
48. Zhu, H., Ownby, D. W., Riggs, C. K., Nolasco, N. J., Stoops, J. K., and Riggs, A. F. (1996) *J. Biol. Chem. 271*, 30007−30021.
49. Wyatt, P. J. (1993) *Anal. Chim. Acta 272*, 1−40.
50. Lyubchenko, Y. L., Gall, A. A., Shlyakhtenko, L. S., Harrington, R. E., Jacobs, B. L., Oden, P. I., and Lindsay, S. M. (1992) *J. Biomol. Struct. Dyn. 10*, 589−606.
51. Lomakin, A., Chung, D. S., Benedek, G. B., Kirschner, D. A., and Teplow, D. B. (1996) *Proc. Natl. Acad. Sci. U.S.A. 93*, 1125−1129.
52. Jarrett, J. T., and Lansbury, P. T., Jr. (1993) *Cell 73*, 1055−1058.
53. Esler, W. P., Stimson, E. R., Jennings, J. M., Vinters, H. V., Ghilardi, J. R., Lee, J. P., Mantyh, P. W., and Maggio, J. E. (2000) *Biochemistry 39*, 6288−6295.
54. Pallitto, M. M., and Murphy, R. M. (2001) *Biophys. J. 81*, 1805−1822.
55. Stine, W. B., Jr., Snyder, S. W., Ladror, U. S., Wade, W. S., Miller, M. F., Perun, T. J., Holzman, T. F., and Krafft, G. A. (1996) *J. Protein Chem. 15*, 193−203.
56. Harper, J. D., Wong, S. S., Lieber, C. M., and Lansbury, P. T., Jr. (1997) *Chem. Biol. 4*, 119−125.
57. Harper, J. D., and Lansbury, P. T., Jr. (1997) *Annu. Rev. Biochem. 66*, 385−407.
58. Shen, C.-L., Scott, G. L., Merchant, F., and Murphy, R. M. (1993) *Biophys. J. 65*, 2383−2395.
59. Murphy, R. M., and Pallitto, M. M. (2000) *J. Struct. Biol. 130*, 109−122.
60. Hilbich, C., Kisters-Woike, B., Reed, J., Masters, C. L., and Beyreuther, K. (1991) *J. Mol. Biol. 218*, 149−163.
61. Sunde, M., Serpell, L. C., Bartlam, M., Fraser, P. E., Pepys, M. B., and Blake, C. C. (1997) *J. Mol. Biol. 273*, 729−739.
62. Serpell, L. C., Sunde, M., Benson, M. D., Tennent, G. A., Pepys, M. B., and Fraser, P. E. (2000) *J. Mol. Biol. 300*, 1033−1039.
63. Burkoth, T. S., Benzinger, T. L. S., Urban, V., Morgan, D. M., Gregory, D. M., Thiyagarajan, P., Botto, R. E., Meredith, S. C., and Lynn, D. G. (2000) *J. Am. Chem. Soc. 122*, 7883−7889.
64. Blackley, H. K. L., Sanders, G. H. W., Davies, M. C., Roberts, C. J., Tendler, S. J. B., and Wilkinson, M. J. (2000) *J. Mol. Biol. 298*, 833−840.
65. Chamberlain, A. K., MacPhee, C. E., Zurdo, J., Morozova-Roche, L. A., Hill, A. O., Dobson, C. M., and Davis, J. J. (2000) *Biophys. J. 79*, 3282−3293.
66. Goldsbury, C., Goldie, K., Pellaud, J., Seelig, J., Frey, P., Muller, S. A., Kistler, J., Cooper, G. J. S., and Aebi, U. (2000) *J. Struct. Biol. 130*, 352−362.
67. Li, L., Darden, T. A., Bartolotti, L., Kominos, D., and Pedersen, L. G. (1999) *Biophys. J. 76*, 2871−2878.
68. Iwata, K., Eyles, S. J., and Lee, J. P. (2001) *J. Am. Chem. Soc. 123*, 6728−6729.
69. Findeis, M. A., Musso, G. M., Arico-Muendel, C. C., Benjamin, H. W., Hundal, A. M., Lee, J. J., Chin, J., Kelley, M., Wakefield, J., Hayward, N. J., and Molineaux, S. M. (1999) *Biochemistry 38*, 6791−6800.
70. Hilbich, C., Kisters-Woike, B., Reed, J., Masters, C. L., and Beyreuther, K. (1992) *J. Mol. Biol. 228*, 460−473.
71. McLaurin, J., and Fraser, P. E. (2000) *Eur. J. Biochem. 267*, 6353−6361.
72. Burkoth, T. S., Benzinger, T. L. S., Jones, D. N. M., Hallenga, K., Meredith, S. C., and Lynn, D. G. (1998) *J. Am. Chem. Soc. 120*, 7655−7656.

BI015985R